

## POLARIMETRY OF DG TAU AT 350 $\mu\text{m}$

M. KREJNY<sup>1,6</sup>, T. G. MATTHEWS<sup>1</sup>, G. NOVAK<sup>1</sup>, J. CHO<sup>2</sup>, H. LI<sup>3</sup>, H. SHINNAGA<sup>4</sup>, AND J. E. VAILLANCOURT<sup>5</sup>

<sup>1</sup> Department of Physics and Astronomy, Northwestern University, 2131 Tech Dr., Evanston, IL 60628, USA; [krejny@astro.umn.edu](mailto:krejny@astro.umn.edu)

<sup>2</sup> Department of Astronomy and Space Science, Chungnam National University, Daejeon, Republic of Korea

<sup>3</sup> Harvard Center for Astrophysics, 60 Garden Street, Cambridge, MA 02138, USA

<sup>4</sup> Caltech Submillimeter Observatory, 111 Nowelo St., Hilo, HI 96720, USA

<sup>5</sup> California Institute of Technology, Division of Physics, Mathematics, and Astronomy, 1200 E. California Blvd., Pasadena, CA 91125, USA

Received 2009 April 27; accepted 2009 September 21; published 2009 October 14

### ABSTRACT

We present the first 350  $\mu\text{m}$  polarization measurement for the disk of the T Tauri star (TTS) DG Tau. The data were obtained using the SHARP polarimeter at the Caltech Submillimeter Observatory. We measured normalized Stokes parameters  $q = -0.0086 \pm 0.0060$  and  $u = -0.0012 \pm 0.0061$ , which gives a  $2\sigma$  upper limit for the percent polarization of 1.7%. We obtain information about the polarization spectrum by comparing our 350  $\mu\text{m}$  measurement with an 850  $\mu\text{m}$  polarization detection previously published for this source. Comparing the two measurements in Stokes space (*not* in percent polarization) shows that the two data points are not consistent, i.e., either the degree of polarization or the angle of polarization (or both) must change significantly as one moves from 850  $\mu\text{m}$  to 350  $\mu\text{m}$ . This conclusion concerning the polarization spectrum disagrees with the predictions of a recent model for TTS disk polarization. We show that this discrepancy can be explained by optical depth effects. Specifically, we demonstrate that if one were to add more mass to the model disk, one would expect to obtain a model polarization spectrum in which the polarization degree falls sharply with increasing frequency, consistent with the observations at the two wavelengths. We suggest that multiwavelength polarimetry of TTS disk emission may provide a promising method for probing the opacity of TTS disks.

*Key words:* polarization – planetary systems: protoplanetary disks – stars: individual (DG Tau) – submillimeter

*Online-only material:* color figure

### 1. INTRODUCTION

T Tauri Stars (TTSs) are low-mass young stellar objects, i.e., objects that have masses similar to that of the Sun and have not yet reached the main sequence. They are characterized primarily by their large infrared excesses that are caused by the dust in their circumstellar disks. TTSs are being studied to learn more about possible first steps in planet formation, e.g., dust coagulation from interstellar medium (ISM) sizes ( $< 1 \mu\text{m}$ ) up to 1 mm. Evidence for grain size growth is found in numerous studies of the millimeter and submillimeter spectral energy distributions (SEDs) of TTSs (e.g., Beckwith & Sargent 1991; Rodmann et al. 2006; Draine 2006). In these studies, the mass opacity index  $\beta$  for TTS disks is found to be generally less than 2, indicative of grain sizes larger than those in the ISM. However, the methods used to determine  $\beta$  require assumptions about the optical depths of the disks. Due to model degeneracies, the results obtained for the grain size, though compelling, are not fully conclusive.

Another property of TTS disk emission that can be observed, besides its SED, is its state of linear polarization. In general, dust grains can produce polarization by any of three mechanisms: thermal emission, selective extinction, and/or scattering. Hildebrand (1988) reviews observations of polarized thermal emission from magnetically aligned interstellar dust grains at far-infrared and submillimeter wavelengths, and shows that one can generally assume that the clouds are optically thin and that selective extinction and scattering are thus negligible (see also Novak et al. 1989; Lazarian 2007). The principal reason for this is that the grain size  $a$  is much smaller than the wavelength  $\lambda$  for these observations. At shorter wavelengths, magnetically

aligned dust grains can produce polarization by selective extinction of starlight, as first seen by Hiltner (1949) and Hall (1949) in the optical, and later observed by others in the near infrared (e.g., Jones et al. 1992). Selective extinction (specifically, selective absorption) has also been seen at far-infrared wavelengths in the unusually dense core of Sagittarius B2 (Dowell 1997). For polarization by scattering, aligned grains are not needed. This mechanism can sometimes produce large polarizations, and has been observed in the optical and NIR (e.g., Werner et al. 1983).

If the dust grains in a TTS disk are aligned, then one should observe polarized millimeter and submillimeter thermal emission. Also, if the grains are growing up to millimeter sizes, then polarization by selective extinction and/or scattering may become non-negligible at millimeter and submillimeter wavelengths. To see why, note that the submillimeter opacity can exceed unity for some large-grain models created for protostellar disks (D'Alessio et al. 2001).

Tamura et al. (1999) were the first to detect polarization in TTS disks in the submillimeter; they detected 850  $\mu\text{m}$  polarization in two approximately edge-on TTS disks. In both cases, the measured polarization magnitude was found to be about 3% and the measured polarization angle was orthogonal to the plane of the disk. They assumed that the polarization mechanism was thermal emission by magnetically aligned dust grains, and on this basis they inferred that the magnetic field orientation for each disk was parallel to the plane of the disk, implying a toroidal magnetic field structure. However, Tamura et al. (1999) did not consider alternative polarization mechanisms, so their conclusions about disk magnetic fields must be considered preliminary. Because the cross sections for scattering and absorption can depend strongly on  $(a/\lambda)$ , measurements of the polarization spectrum of the disk emission may constrain the polarization mechanism. This, in turn, may

<sup>6</sup> Current address: Department of Astronomy, University of Minnesota, 116 Church St. SE, Minneapolis, MN 55455, USA.

**Table 1**  
SHARP 350  $\mu\text{m}$  Observations

Date	Number of Cycles	$\tau_{225\text{GHz}}^a$
2007 Feb 12	11	0.033–0.035
2007 Feb 13	26	0.056–0.066
2007 Feb 14	14	0.062–0.074
2007 Aug 9	4	0.065–0.066
2007 Aug 13	16	0.047–0.049

Note. <sup>a</sup> Zenith atmospheric optical depth measured at 225 GHz.

lead to definitive information about the magnetic field geometry and/or new constraints on the grain size distribution.

In this paper, we present the first 350  $\mu\text{m}$  polarimetric observations of DG Tau, one of the two TTSs studied by Tamura et al. (1999) at 850  $\mu\text{m}$ . The observations were made at the Caltech Submillimeter Observatory (CSO) using SHARP, the SHARC-II Polarimeter (Li et al. 2008). In Section 2, we describe the observations and the analysis, and we present our results. In Section 3 we discuss a model for TTS disk polarization that has recently been published by Cho & Lazarian (2007), and we compare the predictions of this model with initial empirical information on the polarization spectrum of DG Tau derived by comparing our 350  $\mu\text{m}$  measurement with the 850  $\mu\text{m}$  measurement of Tamura et al. (1999).

## 2. OBSERVATIONS, ANALYSIS, AND RESULTS

DG Tau is located in the Taurus-Auriga star formation cloud, at a distance of 140 pc (Beckwith et al. 1990). It has a mass of  $0.6 M_{\odot}$  and luminosity of  $1.7 L_{\odot}$  (Cohen & Kuhl 1979; Beckwith et al. 1990). It is a younger TTS, with an age of approximately  $3 \times 10^5$  yr (Beckwith et al. 1990). DG Tau has a prominent optical jet at a position angle (measured from north to east) of  $226^{\circ}$  (Mundt & Fried 1983), and shows forbidden-line emission, making it a classical TTS.

Disk models created to reproduce the SED suggest a disk mass of  $0.03 M_{\odot}$  (Adams et al. 1990). Based on 2 mm observations, the dust disk is estimated to have a radius of  $109 \pm 22$  AU, and an inclination angle of  $70^{\circ}$ , with  $90^{\circ}$  signifying an edge-on disk (Kitamura et al. 1996). The dust disk is *not* orthogonal to the outflow axis; it is misaligned by almost  $30^{\circ}$ . There is also a large  $^{13}\text{CO}$  gas disk with a major axis of 2800 AU, perpendicular to the optical jet (Sargent & Beckwith 1989; Kitamura et al. 1996).

SHARP is a dual-polarization fore-optics module that adds polarimetric capability to the CSO’s SHARC-II camera (Li et al. 2008). The angular resolution of SHARP at 350  $\mu\text{m}$  is  $\sim 9''$ , so the disk of DG Tau is not resolved. Observations were made during 2007 February 12–14, August 9, and August 13. Table 1 lists observing information. We used chop-nod mode for these observations (Li et al. 2008; Hildebrand et al. 2000). Data were collected in groups of dithers, with one dither consisting of four half-wave plate (HWP) cycles (Hildebrand et al. 2000), each cycle having a slightly different pointing offset. Each cycle had a duration of eight minutes, with data collected at four HWP angles:  $0^{\circ}$ ,  $22.5^{\circ}$ ,  $45^{\circ}$ , and  $67.5^{\circ}$ .

We used the (in-house designed) software programs SHARPINTEG and SHARPCOMBINE to analyze the data. SHARPINTEG processes the individual cycles to yield maps of the unnormalized Stokes Parameters  $I$ ,  $Q$ , and  $U$ . SHARPCOMBINE accepts these maps as inputs and interpolates them onto its own regular equatorial-coordinate grid, with pixel sizes that are half the size of the SHARC-II detector pixels (one “plot pixel” =

$\sim 2.3 \times 2.3$ ). The principles used in this interpolation are described by Houde & Vaillancourt (2007). Interpolation is necessary because of the dithering and the sky rotation (Li et al. 2008), and entails a modest loss of angular resolution. For this process, we used a smoothing kernel having a Gaussian shape of  $9''$  FWHM. The kernel’s cutoff diameter was also set to  $9''$ .

The above procedures have proven reliable in past work, but residual “sky noise” (Hildebrand et al. 2000) or other variations in the radiative load can in principle cause spurious additive signals in both total and polarized flux. Because our target is unresolved by SHARP, our field of view consists mostly of blank sky for which  $I$ ,  $Q$ , and  $U$  should be zero. We have taken advantage of this to remove the kinds of spurious signals described above, by performing the equivalent of synthetic aperture photometry (Howell 2000) on the  $I$ ,  $Q$ , and  $U$  maps that are produced by SHARPCOMBINE. The effect of this process is to remove any “DC offsets” in flux and/or polarized flux that are uniform across the array. For each of the three maps ( $I$ ,  $Q$ , and  $U$ ), we defined an annulus centered on the central pixel of the map (the location of DG Tau), calculated a (straight) average over the annulus pixels, and then subtracted this average value (the DC offset) from the value determined at the center pixel. The inner radius of the annulus was chosen to be twice the kernel diameter; this ensured that SHARPINTEG output values used to compute the central SHARPCOMBINE output pixel would not also be used to compute the DC offset, and visa versa. The outer radius was chosen to give a total number of pixels that was 10 times that of the kernel; larger choices resulted in inclusion of parts of the SHARPCOMBINE maps having lower sampling, resulting in larger noise levels. The annulus had a total sky coverage corresponding approximately to that of one instantaneous pointing of the  $12 \times 12$  pixel ( $55'' \times 55''$ ) polarimetry array of SHARP. Our use of synthetic aperture photometry is illustrated in Figure 1.

From the final values of  $I$ ,  $Q$ , and  $U$  for DG Tau, and the associated statistical errors, normalized Stokes parameters ( $q = Q/I$  and  $u = U/I$ ) were then calculated to obtain our final result. (We also apply the usual corrections for instrumental polarization and polarimetric efficiency, as detailed in Li et al. 2008.) Note that in SHARPINTEG and SHARPCOMBINE, errors are propagated from the short-timescale errors determined from each nod, as described by Hildebrand et al. (2000), Kirby et al. (2005), and references therein. In order to assess the effects of systematic error on our results, we processed the data a second time, but with the data grouped into seven temporal bins. SHARPCOMBINE  $I$ ,  $Q$ , and  $U$  maps were created separately for each bin, and DC values derived from annuli were subtracted from the  $I$ ,  $Q$ ,  $U$  values measured at the centers of these maps, for each of the bins. The purpose of the binning was to determine the reduced chi squared ( $\chi_{\text{red}}^2$ ) of the  $q$  and  $u$  data, which may be compared to that obtained without the DC offset subtraction. We found that the offset subtraction lowered  $\chi_{\text{red}}^2$  from 1.5 and 1.6 to 0.9 and 0.8 (for  $q$  and  $u$ , respectively). Thus, after the DC offset subtraction, the data appear to be free from systematic error. We found that the  $q$  and  $u$  values obtained via the two methods (averaging of all files in one bin versus using seven bins and taking a weighted average over results for individual bins) are very consistent. We adopt the values from the first method as our final result, which are  $q = -0.0086 \pm 0.0060$  and  $u = -0.0012 \pm 0.0061$ .

Finally, we note that in examining the  $I$  maps we found a small amount of flux from DG Tau,  $\sim 2\%$ , contaminating the annulus (see upper right panel in Figure 1). However, this flux should be consistent across all Stokes parameters. If 0.98 of the flux for

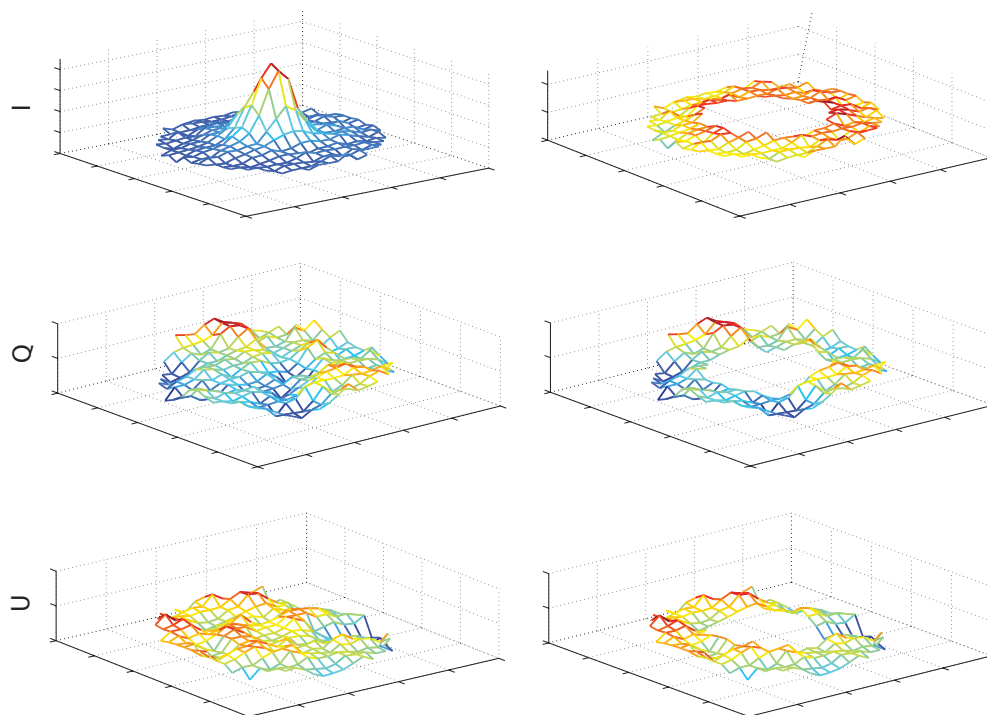


**Figure 1.** SHARPCOMBINE output maps of  $I$ ,  $Q$ , and  $U$  for DG Tau. The left panels show the full maps, with only the outermost high-noise regions removed, while the right panels show only the portion of each map that is used for computing the DC offset, i.e., the annulus regions. The range of values encompassed by the vertical scale, in arbitrary flux units, is approximately  $-2.0$  to  $+7.0$  for the full  $I$  map,  $-2.0$  to  $+2.0$  for the annulus  $I$  map, and  $-0.2$  to  $+0.2$  for all other maps.

(A color version of this figure is available in the online journal.)

each Stokes parameter remains after the DC offset subtraction, then this factor should cancel out upon determination of the normalized Stokes parameters  $q$  and  $u$ .

### 3. DISCUSSION

#### 3.1. The Model of Cho & Lazarian

Cho & Lazarian (2007) present a model for polarized thermal emission from magnetically aligned grains in a TTS disk. Besides treating polarized emission, their model naturally incorporates the effects of large absorption optical depths. The model does not include the effects of polarization by scattering, as they determine from simple estimates (discussed at the end of this section) that thermal emission is the dominant polarization mechanism.

Cho & Lazarian (2007) use a flared, two-layered (surface and interior) disk model, incorporating a distribution of grain sizes extending up to 1 mm. The disk is permeated by a regular, toroidal magnetic field, and the model predicts that the submillimeter/millimeter emission should be polarized in a direction orthogonal to this field, giving polarization perpendicular to the disk plane for a TTS disk viewed approximately edge-on.

In the Cho & Lazarian (2007) model, the degree of grain alignment in the disk is calculated under the assumption that grains are brought into alignment with the magnetic field via the radiative torque mechanism. A simple scaling law taken from Cho & Lazarian (2005) is used to estimate the radiative torque efficiency, and then the degree of alignment is calculated from this following the methods of Draine & Weingartner (1996). The result is that the degree of alignment depends on the grain size, the local radiation environment, and the local gas density. The

radiative torque efficiency is high when  $(\lambda/a)$  is near unity ( $\lambda$  and  $a$  are the characteristic wavelength of the ambient radiation and the grain size) and falls rapidly as this ratio increases. We note that the simple grain alignment model used in Cho & Lazarian (2007) does not take into account the possibility of alignment at low- $J$  attractor points nor the dependence of the alignment on the angle between the radiation and the magnetic field (Lazarian & Hoang 2007; Hoang & Lazarian 2009). One result of the Cho & Lazarian (2007) model is that grain alignment is generally better at larger distances from the star. This is caused in part by the fact that there is higher gas density closer to the star. Another result is that for the disk interior there is preferential alignment of larger grains, since the grains in the interior see primarily longer-wavelength radiation.

In the Cho & Lazarian (2007) model, many factors affect the degree of polarization of the grains' emission, including of course the degree of grain alignment and the axis ratio of the grains (assumed to be oblate spheroids). One additional factor that affects the polarization is the absorption optical depth, which for some wavelengths and sight-lines can approach or exceed unity. In these cases, the calculated polarization will tend to be suppressed. This is because the polarization by absorption that the grains near the front of the disk impress upon the radiation from the grains near the back of the disk is orthogonal to the intrinsic polarization of that radiation. This effect is also discussed by Hildebrand et al. (2000), and we shall refer to it as *polarization self suppression*, or PSS.

Cho & Lazarian (2007) find that the disk interior becomes optically thick for  $\lambda < 100 \mu\text{m}$ , while the surface layer remains optically thin. The hotter surface grains dominate the mid-IR polarization, while the cooler interior dust grains dominate polarization in the far-infrared/submillimeter. Because the grain temperature falls with increasing distance from the star,

the shorter (longer) wavelength measurements preferentially sample grains at smaller (larger) distances from the star.

In their Figure 12, Cho & Lazarian (2007) show predicted polarization spectra for unresolved disks at various inclination angles  $i$ . Note that as  $i$  approaches zero (face-on view), the polarization also approaches zero, for all wavelengths. This is due to polarization cancellation, as the disk's polarization pattern becomes radial for  $i = 0^\circ$ .

Finally, we review the discussion of polarization by scattering in Cho & Lazarian (2007). For ISM sized grains, far-infrared/submillimeter scattering cross sections are negligible, but this is not necessarily true for large,  $1000 \mu\text{m}$  grains. Cho & Lazarian (2007) carried out a simple calculation to estimate the relative importance of polarization by scattering versus polarization by thermal emission. They chose a point in the midplane of the disk, and calculated both the scattered flux  $F_{\text{sca}}$  and the flux from the thermally emitting dust grains,  $F_{\text{em}}$ . The polarized flux due to scattering is proportional to the first of these two quantities while that due to thermal emission is proportional to the second. Figure 16 of Cho & Lazarian (2007) plots the ratio of scattered flux to thermal emission  $F_{\text{sca}}/F_{\text{em}}$  as a function of disk radius. For submillimeter wavelengths, the ratio is less than unity, except at small radii. Since the submillimeter polarization is dominated by the outer part of the disk, the authors conclude that polarization by scattering is not dominant at these long wavelengths. We note that this conclusion is based on a crude approximation, as it assumes that the percent polarization for polarization by scattering is less than or equal to that for polarization by thermal emission (which may not be true).

### 3.2. Comparing the Observations to Model Predictions

The  $q$  and  $u$  values for the measured  $350 \mu\text{m}$  polarization (see Section 2) give a percent polarization of  $P_{350 \mu\text{m}} = 0.9\% \pm 0.6\%$ . Using the results of Vaillancourt (2006) as plotted in his Figure 3(a), we calculate a  $2\sigma$  upper limit of  $1.7\%$ . The degree of polarization reported by Tamura et al. (1999) at their longer wavelength is  $P_{850 \mu\text{m}} = 2.95\% \pm 0.89\%$ .  $P_{350 \mu\text{m}}$  and  $P_{850 \mu\text{m}}$  agree within  $2\sigma$ . However, Figure 2 plots the  $850 \mu\text{m}$  measurement together with our  $350 \mu\text{m}$  measurement in Stokes space, with circles that denote 1 and  $2\sigma$  error bars, and it can be seen that the Stokes parameters corresponding to the measurements at the two wavelengths do not agree within  $2\sigma$ ; the  $2\sigma$  error-circles do not overlap. Thus, the two measurements taken together imply significant structure in the polarization spectrum, i.e., either the degree of polarization or the angle of polarization (or both) must change as one moves from  $850 \mu\text{m}$  to  $350 \mu\text{m}$ .

The vertically cross-hatched portion of the Stokes plot in Figure 2 represents the locus of points that are consistent with polarization oriented orthogonal to the plane of the disk within the errors given by Kitamura et al. (1996). For this purpose, the position angle of the disk axis was taken to be  $99^\circ \pm 10^\circ$  (Kitamura et al. 1996). As we noted in Section 1, the  $850 \mu\text{m}$  point is consistent with polarization orthogonal to the disk. Our  $350 \mu\text{m}$  measurement is barely consistent with this polarization orientation, and is consistent within  $2\sigma$  with zero. If we assert, following Tamura et al. (1999) and Cho & Lazarian (2007), that the submillimeter polarization is oriented perpendicular to the plane of the disk, then the measurements shown in Figure 2 indicate that the polarization must drop by at least a factor of 2 or 3 as one moves from  $850 \mu\text{m}$  to  $350 \mu\text{m}$ .

We compare this result to the submillimeter polarization spectrum predicted by Cho & Lazarian (2007) for an unresolved disk viewed at a  $60^\circ$  inclination angle, which is plotted in the

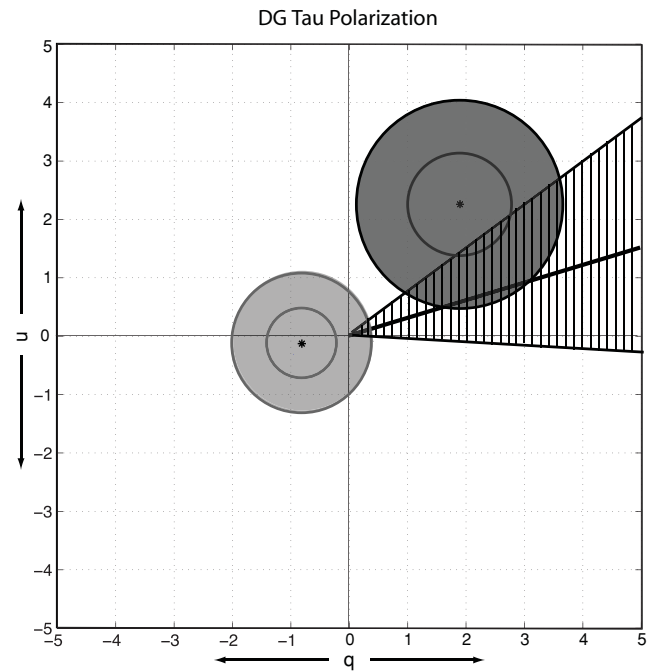


**Figure 2.** Plot in Stokes space of Tamura et al. (1999)  $850 \mu\text{m}$  polarization measurement (dark gray circle, first quadrant) together with our  $350 \mu\text{m}$  measurement (light gray circle, third quadrant). Stokes  $q$  and  $u$  are plotted in percent. Circles signify  $1\sigma$  and  $2\sigma$  errorbars. The two measurements do not agree within  $2\sigma$ , indicating structure in the polarization spectrum. In other words, either the degree of polarization or the angle of polarization (or both) must change as one moves from  $850 \mu\text{m}$  to  $350 \mu\text{m}$ . The vertically hatched region denotes the locus of points that are consistent with polarization orientated orthogonally to the plane of the disk. (The disk is at position angle  $99 \pm 10^\circ$ .) The  $850 \mu\text{m}$  point is consistent with polarization perpendicular to the disk plane; the  $350 \mu\text{m}$  measurement is consistent with zero.

upper right panel of their Figure 12. (This inclination angle is the plotted angle closest to that of DG Tau; see Section 2.) As can be seen in this polarization spectrum, the degree of polarization is reasonably flat across the submillimeter bands; from the original numerical data used by Cho & Lazarian (2007) to make this plot we find that the ratio of  $850$  to  $350 \mu\text{m}$  polarization ( $P_{850}/P_{350}$ ) is 1.28. This disagrees with the observations.

One possible difference between the model disk and the actual DG Tau disk is the mass; the model disk's mass is  $0.014 M_\odot$ , while the mass of the DG Tau disk has been estimated to lie in the range  $0.02$ – $0.06 M_\odot$  (Kitamura et al. 1996; Beckwith & Sargent 1991; Mannings & Emerson 1994). Increasing the mass of a disk increases the optical depth along any line of sight through the disk. Recall that large optical depth can reduce polarization via the PSS effect Section 3.1. Is it possible that the difference between the model disk's polarization spectrum and that of the real DG Tau disk is due to suppression of the  $350 \mu\text{m}$  polarization in the real disk via a PSS effect induced by the extra optical depth? To answer this question conclusively, we would have to redo the theoretical work, exploring larger mass values. However, a preliminary answer can be obtained via extrapolations based on information extracted from Cho & Lazarian (2007). Specifically, we will explore the role of optical depth and PSS in their  $0.014 M_\odot$  disk.

First note, however, that the PSS effect must be more severe at shorter wavelengths if it is to cause the observed drop in polarization moving from  $850 \mu\text{m}$  to  $350 \mu\text{m}$ . The frequency dependence of the mass opacity  $\kappa_\nu$ , which is defined as the optical depth  $\tau$  divided by the mass column density, is generally taken to be  $\kappa_\nu \propto \nu^\beta$  (e.g., see Stahler & Palla 2004). Since the

mass column density has no wavelength dependence, we must have  $\tau \propto \nu^\beta$  as well. For TTS disks,  $\beta$  is usually less than 2 in the submillimeter but is rarely negative (see references given in Section 1). This implies that, for a given line of sight and a given dust distribution,  $\tau$  decreases with increasing wavelength. Thus, the PSS effect should indeed be more significant for our 350  $\mu\text{m}$  measurement than for 850  $\mu\text{m}$ .

Turning to the question of the role of optical depth and PSS in the 0.014  $M_\odot$  disk of Cho & Lazarian (2007), we next consider the right-hand panel of their Figure 13, which plots the degree of polarization versus inclination angle for a selection of far-infrared/submillimeter wavelengths. These plots only consider polarization for the disk interior; for now we shall neglect the surface layers. From the original numerical data used by Cho & Lazarian (2007), we find that the ratio of 100 and 850  $\mu\text{m}$  polarization at an inclination  $i = 70^\circ$  is  $(P_{100}/P_{850}) = 0.15$ . It is reasonable to ask whether this large drop in polarization from 850  $\mu\text{m}$  to 100  $\mu\text{m}$  is caused by PSS, or is an intrinsic feature of the disk which could result from the fact that the grains that produce polarization at the shorter wavelength reside in warmer regions closer to the star, and are thus less aligned (see Section 3.1).

This question is resolved when we compare this polarization ratio to values obtained for lower inclination angles. For  $i = 30^\circ$ , the data used to make the right-hand panel of Figure 13 of Cho & Lazarian (2007) give  $(P_{100}/P_{850}) = 0.39$ . Since the polarization pattern observed becomes centrosymmetric for small inclination angles, the polarization tends to cancel as  $i$  approaches zero. This is a purely geometric effect, unrelated to optical depth, so this polarization cancellation should affect the polarization observed at all wavelengths equally, and the polarization ratio should therefore not change with inclination angle. However, we see that the ratio of polarization changes very significantly with inclination. This is in accord with the expected behavior of PSS, because (a) as one increases the optical depth along the line of sight by increasing  $i$  the PSS should get stronger, and (b) the PSS should have a more significant effect at 100  $\mu\text{m}$  than at 850  $\mu\text{m}$ . We conclude that the dramatic change in polarization between 100  $\mu\text{m}$  and 850  $\mu\text{m}$  for  $i = 70^\circ$  (for the disk interior) is due in large part to PSS. The effect of PSS should not be as dramatic at longer wavelengths, which is confirmed by studying the 350  $\mu\text{m}$ /850  $\mu\text{m}$  polarization ratio; at  $i = 70^\circ$  the ratio is 0.72, and it only increases to 0.83 at  $i = 30^\circ$ .

As discussed above, the disk mass used by Cho and Lazarian differs from the presumed DG Tau value by a factor of 1.4–4.0. If one were to repeat the work of Cho & Lazarian (2007) using a disk mass that is higher than the one they used by a factor in this range then the effects of PSS would certainly get worse, and the dramatic PSS effects that we see in the 0.014  $M_\odot$  disk at 100  $\mu\text{m}$  might begin to move into the submillimeter. It seems plausible that the value of the ratio  $(P_{350}/P_{850})$  for the  $i = 70^\circ$  case (this value of  $i$  matches the actual DG Tau disk; see Section 2) could then decrease from 0.72, which was found for the 0.014  $M_\odot$  disk, to a value below 0.5 which would match the observations. Note that, as mentioned previously, this discussion neglects the surface layers, which do emit polarized light. However, as noted in Section 3.1, for submillimeter wavelengths, the surface layers do not contribute significantly to the total polarization.

One alternative explanation for the discrepancy between the predicted and observed polarization spectra is polarization by scattering. As we discussed in Section 3.1, Cho & Lazarian (2007) argue that scattering is less important than polarized emission in the submillimeter. However, this argument is based

only on a rough estimate of the ratio of scattered to emitted flux. Furthermore, while they do find that the ratio  $(F_{\text{sca}}/F_{\text{em}})$  is less than unity for radii corresponding to the outer disk, where the submillimeter radiation originates, this ratio nonetheless does hover near 0.5 over much of the relevant range. A disk having a larger mass will have scattering optical depths exceeding unity out to relatively larger disk radii, in comparison with a lower-mass disk. Thus, it is likely that if one were to repeat the analysis given in Cho & Lazarian (2007) using a larger-mass disk, the importance of scattering would be found to be greater. Would the scattering mechanism give a polarization that falls sharply as one moves shortward in wavelength from 850 to 350  $\mu\text{m}$ ? Cho & Lazarian (2007) do not evaluate the spectrum for this polarization mechanism, but crude toy models by Krejny (2008) suggest that indeed we should expect a polarization that falls with increasing frequency for this waveband.

Finally, we discuss a third explanation for the structure seen in Figure 2. We note that the location of our 350  $\mu\text{m}$  polarization point overlaps with the locus of points corresponding to polarization parallel to the plane of the disk (although it is important to note that we have not obtained even a  $2\sigma$  detection). It is possible that this is indicative of a change in magnetic field direction. As the observing wavelength decreases, the observed radiation probes dust grains having higher temperatures. (Here we are assuming polarization by emission, not scattering.) Thus it is possible that our 350  $\mu\text{m}$  measurement is sampling a warmer collection of grains, located closer to the central star. In this case, our result may indicate a change in the magnetic field geometry with radius; the low polarization at 350  $\mu\text{m}$  may indicate a chaotic field. It is difficult to evaluate the plausibility of this explanation for the observed structure in the polarization spectrum. But the first two explanations discussed in this section (namely, PSS and polarization by scattering) naturally account for a polarization that drops with increasing frequency which is suggested by the observations. Specifically, PSS is expected to be worse at high frequency (see above), and polarization by scattering is expected to be lower at the shorter submillimeter wavelengths, judging from toy models (Krejny 2008).

In summary, when we compare our 350  $\mu\text{m}$  polarization measurement to the 850  $\mu\text{m}$  measurement of Tamura et al. (1999), we see evidence for significant structure in the polarization spectrum. This is inconsistent with the model of Cho & Lazarian (2007) which gives polarization perpendicular to the disk, with similar polarization magnitudes at the two wavelengths. We have proposed three possible explanations for the discrepancy, and we believe the first two are more natural. For these two favored explanations, the discrepancy arises as a consequence of the larger mass of the DG Tau disk in comparison with the model disk. The first explanation is PSS at 350  $\mu\text{m}$  due to the larger absorption optical depth of a more massive disk, and the second is the onset of polarization by scattering, considered negligible by Cho & Lazarian (2007) for their lower-mass disk.

If either of our two preferred explanations is correct, then the submillimeter polarization spectrum of DG Tau is determined by optical depth effects, either absorption optical depth, scattering optical depth, or both. In this case, future multiwavelength polarimetry of TTS disk emission, e.g. with SOFIA, ALMA, and EVLA, may constrain the optical depth which is an important unknown in TTS research.

We thank A. Lazarian, and B. Whitney for their comments and suggestions. For help with the development and commissioning of SHARP, we are grateful to M. Houde, M. Attard,

R. Hildebrand, L. Kirby, C. D. Dowell, and L. Leeuw. This work was supported by the NSF via grants AST 02-41356 and AST 05-05230 to Northwestern University. Additional support came in the form of a NASA GSRP Award to M.K. The CSO is supported by NSF grant AST 05-40882.

*Facilities:* CSO (SHARP)

#### REFERENCES

- Adams, F. C., Emerson, J. P., & Fuller, G. A. 1990, *ApJ*, **357**, 606  
 Beckwith, S. V. W., & Sargent, A. I. 1991, *ApJ*, **381**, 250  
 Beckwith, S. V. W., Sargent, A. I., Chini, R. S., & Guesten, R. 1990, *AJ*, **99**, 924  
 Cho, J., & Lazarian, A. 2005, *ApJ*, **631**, 361  
 Cho, J., & Lazarian, A. 2007, *ApJ*, **669**, 1085  
 Cohen, M., & Kuhl, L. V. 1979, *ApJS*, **41**, 743  
 D'Alessio, P., Calvet, N., & Hartmann, L. 2001, *ApJ*, **553**, 321  
 Dowell, C. D. 1997, *ApJ*, **487**, 237  
 Draine, B. T. 2006, *ApJ*, **636**, 1114  
 Draine, B. T., & Weingartner, J. C. 1996, *ApJ*, **470**, 551  
 Hall, J. S. 1949, *Science*, **109**, 166  
 Hildebrand, R. H. 1988, *QJRAS*, **29**, 327  
 Hildebrand, R. H., Davidson, J. A., Dotson, J. L., Dowell, C. D., Novak, G., & Vaillancourt, J. E. 2000, *PASP*, **112**, 1215  
 Hiltner, W. A. 1949, *Science*, **109**, 165  
 Hoang, T., & Lazarian, A. 2009, *ApJ*, **697**, 1316  
 Houde, M., & Vaillancourt, J. E. 2007, *PASP*, **119**, 871  
 Howell, S. B. 2000, Handbook of CCD Astronomy (Cambridge Observing Handbooks for Research Astronomers; New York: Cambridge Univ. Press)  
 Jones, T. J., Klebe, D., & Dickey, J. M. 1992, *ApJ*, **389**, 602  
 Kirby, L., Davidson, J. A., Dotson, J. L., Dowell, C. D., & Hildebrand, R. H. 2005, *PASP*, **117**, 991  
 Kitamura, Y., Kawabe, R., & Saito, M. 1996, *ApJ*, **465**, L137  
 Krejny, M. 2008, PhD thesis, Northwestern Univ.  
 Lazarian, A. 2007, *J. Quant. Spectrosc. Radiat. Transfer*, **106**, 225  
 Lazarian, A., & Hoang, T. 2007, *MNRAS*, **378**, 910  
 Li, H., Dowell, C. D., Kirby, L., Novak, G., & Vaillancourt, J. E. 2008, *Appl. Opt.*, **47**, 422  
 Mannings, V., & Emerson, J. P. 1994, *MNRAS*, **267**, 361  
 Mundt, R., & Fried, J. W. 1983, *ApJ*, **274**, L83  
 Novak, G., Gonatas, D. P., Hildebrand, R. H., Platt, S. R., & Dragovan, M. 1989, *ApJ*, **345**, 802  
 Rodmann, J., Henning, T., Chandler, C. J., Mundy, L. G., & Wilner, D. J. 2006, *A&A*, **446**, 211  
 Sargent, A. I., & Beckwith, S. V. W. 1989, in Lecture Notes in Physics, Vol. 350, IAU Colloq. 120: Structure and Dynamics of the Interstellar Medium, ed. G. Tenorio-Tagle, M. Moles, & J. Melnick (Berlin: Springer), 215  
 Stahler, S. W., & Palla, F. 2004, The Formation of Stars (Weinheim: Wiley-VCH)  
 Tamura, M., Hough, J. H., Greaves, J. S., Morino, J. I., Chrysostomou, A., Holland, W. S., & Momose, M. 1999, *ApJ*, **525**, 832  
 Vaillancourt, J. E. 2006, *PASP*, **118**, 1340  
 Werner, M. W., Capps, R. W., & Dinerstein, H. L. 1983, *ApJ*, **265**, L13